LATTICE BOLTZMANN SIMULATION OF MELTING PHENOMENON WITH NATURAL CONVECTION FROM AN ECCENTRIC ANNULUS

by

Mahmoud JOURABIAN, Mousa FARHADI *, Ahmad Ali RABIENATAJ DARZI, and Abbas ABOUEI

Faculty of Mechanical Engineering, Babol University of Technology, Babol, I. R. of Iran

Original scientific paper
DOI: 10.2298/TSCI110510012J

In the present study, a double-population thermal lattice Boltzmann method was applied to solve phase change problem with natural convection in an eccentric annulus. The simulation of melting process from a concentrically and eccentrically placed inner hot cylinder inside an outer cold cylinder with Prandtl number of 6.2, Stefan number of 1, and Rayleigh number of 10^5 was carried out quantitatively. It was found that the position of the inner cylinder inside the outer cylinder significantly influence the flow patterns including the size and shape of two formed vortexes. It is also observed that the maximum of liquid fractions occurs where the inner cylinder is mounted at the bottom of outer cylinder.

Key words: *lattice Boltzmann method, melting, solid-liquid phase change, Bhatangar-Gross-Krook collision, natural convection, phase change material*

Introduction

Numerical modeling of transport phenomenon associated with phase change (melting and solidification) has continued to be a significant research area, owing to the fact that melting plays an important role in many industrial applications, such as welding, metal casting, and thermal energy storage (TES).

Investigation of melting process with natural convection in a rectangular cavity has been conducted experimentally [1-3], theoretically [4-5], and numerically [6-7].

Similar to this study, many papers have concentrated on the melting of phase change materials (PCM) that are encapsulated in an annulus as a more sophisticated model for latent heat thermal storage systems (LHTSS). Free convection-controlled melting of a PCM inside a cylindrical-horizontal annulus was simulated numerically by Ng *et al.* [8]. It was concluded that by increasing the Rayleigh number the melting rate was augmented. Furthermore, melting of PCM in the bottom half of the annulus was very ineffective because most of the charged energy was transferred to the top half of the annulus by the convective flow. Betzel and Beer [9] investigated melting and solidification processes of an unfixed PCM encapsulated in a horizontal concentric annulus by experimental methods and a combined analytical and numerical techniques. In the melting process, thin liquid film appeared between the un-melted PCM and the heated walls and the conduction played the main mode of heat transfer. At the upper positions convection heat transfer caused melting although the melting rates were small. Convection melting of a pure PCM encapsulated in a concentric horizontal annulus with two different configurations was investigated numerically by Khillarkar *et al.* [10]. Liu *et al.* [11] examined experimentally

* Corresponding author; e-mail: mfarhadi@nit.ac.ir

melting processes of stearic acid in an annulus enhanced by inserting fins. Experimental and numerical study of paraffin wax melting in the annulus of two coaxial cylinders was carried out by Dutta *et al.* [12]. It was said the convection heat transfer dominated in the melting phase and the eccentricity played a key role for the net circulation of the liquid phase. Tombarevic and Vusanovic [13] performed the numerical modeling of ice melting in horizontal cylindrical annulus using modified enthalpy method. The influence of inner pipe temperature on the shape of phase change front, melting rate and flow and temperature fields was studied. Numerical study of melting of N-eicosane inside a horizontal annulus was carried out by Rabienataj *et al*. [14]. Results showed that the conduction was prevailing at the early stages of process. However, after some elapsed times, convective heat transfer dominated at top half of annulus while conduction heat transfer remained prevailing in the bottom of heated cylinder.

In the solid-liquid phase change problem, the complex coupling which exists between the fluid flow and the moving boundary determines the exact position of solid-liquid interface. In order to overcome this difficulty, different schemes have been suggested in the literature. Bertrand *et al.* [15] utilized the front-tracking method for an easy problem where phase change is driven by laminar thermal convection in the melt. They found that this method is better adapted for a problem of fusion of a pure substance. The level set method is a different method to deal with solid-liquid interface and to avoid the asymptotic analysis used in phase field models. To explicitly track the interface growth, Tan and Zabaras [16] applied a front tracking approach based on the level set method. The adaptive grid method is another way that has been successfully examined for simulation of viscous and inviscid flows by Jin and Xu [17]. They found that for unsteady flow computation, the use of adaptive mesh has obvious advantage in terms of the accuracy and efficiency in comparison with the methods with static mesh points. Boettinger *et al.* [18] employed the phase-field method for modeling of solidification. This method applies a phase-field variable and a corresponding governing equation which describe, respectively, location of a liquid or solid node and state in a material as a function of position and time. It is significant to know that governing equations for the heat and solute can be also solved without tracking the liquid-solid interface.

In recent years, methods based on lattice Boltzmann equation (LBE) has recently become an alternative for simulating fluid flows in channels [19], curved boundaries [20-23], nanofluids [24, 25], and phase-change [26-31]. Unlike conventional computational fluid dynamics (CFD) methods based on the discretization of macroscopic continuum equations, the LBE method is based on microscopic models and mesoscopic kinetic equations in which the combined behavior of the particles is applied to simulate the physical mechanism of the systems. Following improvements can be found in the utilization of lattice Boltzmann methods (LBM): (1) ability to handle interfacial dynamics and intricate moving geometries due to their kinetic nature, (2) a comparably straightforward explicit algorithm on the uniform grids, and (3) an easy computer implementation with fast computational speed, and so on.

There are two LBM for solving of solid-liquid phase transitions: first, phase-field method based on Ginzburg-Landau's theory [32-35] and second, enthalpy-based method [36].

By implementing an enthalpy method, the solid-liquid phase change problems become much simpler because: (1) the governing equations are identical for the solid and liquid phases, (2) there is no need to satisfy boundary condition at the phase change front, (3) it creates a mushy zone that prevents sharp discontinuities, and (4) the position of solid-liquid interface can be ascertained by using the temperature field.

Chatterjee and Chakraborty [37] formulated a D3Q15 lattice model for solving heat diffusion problem coupled with phase change. An adapted latent heat method is incorporated

with LBE for precisely predicting the liquid fractions during the evolution of phase change front. Chatterjee and Chakraborty [38] also developed a hybrid lattice Boltzmann model (LB) model for handling conduction solidification in a single-component configuration. By incorporating enthalpy method with heat conduction equation Jiaung *et al*. [36] developed a LBE for solving solid-liquid phase change problem. Semma *et al.* [27] used LBM to solve Rayleigh-Benard (RB) problem with phase change. The phase change interface was treated as a porous media. They suggested that such a scheme can be simply implemented in simulation of local micro-flows and local solidification structures in 3-D systems. Ganaoui and Semma [28] developed a hybrid scheme based on the coupling between LBM and finite volume method (FVM). They assumed that the solid-liquid phase change front can be handled as a curve boundary condition. It was concluded that the size of melted zone enhances with time although the number of recirculating vortexes declines. A general LB study about conduction and convection melting was carried out by Huber *et al.* [39]. A lot of different diagrams such as dimensionless temperature, melting front position, average Nusslet number and temperature contours *vs.* dimensionless times such as Ste × Fo or Fo were provided. They also show that the proposed model allows a study of natural convection melting in porous medium.

Consequently, the aim of the present work is to numerically investigate melting phenomenon in a cylindrical-horizontal annulus filled with ice (water). In this research study, we choose the multi distribution function (MDF) approach that LBM presents for handling multi-physics problems. To validate convection melting consequences in a square cavity, liquid fraction and average Nusselt number on the hot wall are compared with the Huber *et al.* [39] work for Pr = 1, Ste = 10, and Ra = $1.7 \cdot 10^6$. Also, the effect of different positions of inner cylinder on the flow patterns and melting rates is studied for Ra of 10^5, Pr of 6.2, and Ste of 1. The details of computational procedures are discussed in the following sections.

Mathematical description and governing equations

The representative schematic of computational domain is shown in fig. 1. It consists of two eccentric cylinders that inner and outer cylinders have radius of r and R, respectively. The space between these two cylinders is filled with a solid material and kept at the temperature of T_0. In this case, because the sub-cooling case is neglected, T_0 is equal to melting temperature T_m. The inner cylinder is held at the temperature of $T_1 (T_1 > T_0)$, while the outer cylinder is maintained at the temperature of T_0. The radius ratio *rr* between the inner and outer cylinder is fixed at 3.3.

The different positions of the inner cylinder inside the outer cylinder are chosen to reveal the dependence of heat transfer and fluid flow behaviour on eccentricity (tab. 1).

Based on the assumptions that the liquid phase is regarded as an incompressible fluid, the Boussinesq approximation is adapted for numerical computation, the properties of solid and liq-

Table 1. The dimensionless position of center of inner cylinder within the outer cylinder

	Top	Center	Left	Left and bottom	Bottom
$X_r = \frac{x_r}{R}$	0	0	–0.5	–0.35	0
$Y_r = \frac{y_r}{R}$	0.5	0	0	–0.35	–0.5

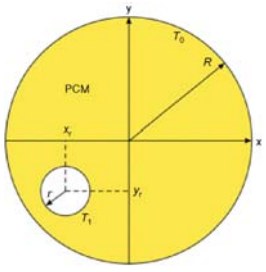

Figure 1. Representative schematic of computational domain

uid phases are constant, no volumetric change is occurred as the phase change takes place, and the compression work done by the pressure and viscous heat dissipation are neglected, the governing equations can then be derived as [27]:

$$\nabla u = 0 \tag{1}$$

$$\frac{\partial u}{\partial t} + u(\nabla u) = -\nabla p + v\nabla^2 u - g\beta(T - T_0) \tag{2}$$

$$\frac{\partial T}{\partial t} + u(\nabla T) = \alpha\nabla^2 T - \frac{L_f}{\rho c_p}\frac{\partial F_l}{\partial t} \tag{3}$$

in which, p is the pressure and c_p – the heat capacity. The governing equations of the melting process with natural convection can be expressed in the dimensionless form as [39, 40]:

$$\nabla u^* = 0 \tag{4}$$

$$\frac{\partial u^*}{\partial t^*} + u^*(\nabla u^*) = -\nabla p^* + \mathrm{Pr}\nabla^2 u^* - \mathrm{Pr}\,\mathrm{Ra}\beta T^* \tag{5}$$

$$\frac{\partial T^*}{\partial t^*} + u^*(\nabla T^*) = \nabla^2 T^* - \frac{1}{\mathrm{Ste}}\frac{\partial F_l}{\partial t^*} \tag{6}$$

The following dimensionless parameters are:

$$T^* = \frac{T - T_0}{T_1 - T_0},\ \mathrm{Fo} = t^* = \frac{t\alpha}{l^2},\ x^* = \frac{x}{l},\ y^* = \frac{y}{l} \tag{7}$$

Here β and g are the thermal expansion coefficient and the acceleration due to gravity force, respectively and l is the appropriate length scale of the system and is equivalent to $2(R - r)$.

Lattice Boltzmann method

LBM [41-43] provides a mesoscopic description of the transport properties of physical systems. It is a powerful technique for the computational modelling of a wide variety of complex fluid flow problems including single and multiphase flow in the complex geometries. The LBE [43] is a minimal form of the Boltzmann kinetic equation and is a simple evolution equation for a particle distribution function f (x, c, t), which represents the probability to find a particle at the lattice position x and time t, moving with the speed of c. According to the theory of the LBM, it consists of two steps: collision and streaming. In the collision step, the particle distribution functions (PDF) for each direction are relaxed toward quasi-equilibrium distributions. Afterward, at the streaming step, the particles move to the neighbouring points according to their (discrete) velocity. Therefore, the PDF alternates between particle streaming and collision.

LBE for the velocity field

The first point of the LBM is the kinetic equation for PDF along the i^{th} direction, $f_i(x, t)$ [26, 27]:

$$f_i(x + c_i\Delta t, t + \Delta t) - f_i(x, t) = \Omega_i[f(x, t)] \tag{8}$$

Here Ω_i is the linearized collision operator which represents the local change in the particle distribution due to the collision between particles. In the LBM development, an important simplification is to approximate the collision operator with the so called Bhatangar-Gross-Krook (BGK) single relaxation time approximation [43]. The lattice BGK equation can then be written as [26, 27]:

$$f_i(x + c_i\Delta t, t + \Delta t) - f_i(x, t) = -\frac{f_i(x, t) - f_i^{eq}(x, t)}{\tau} + \Delta t\vec{c}_i F_i \tag{9}$$

where f_i^{eq}, the equilibrium PDF is approximated by a polynomial of macroscopic properties and is derived from conservation laws and τ is the rate at which the distribution function f_i relaxes to f_i^{eq}. F_i is the body force that donates the buoyancy force vector. In order to formulate buoyancy force in the natural convection problem, the Boussinesq approximation was applied and the radiation heat transfer was neglected. Thus, the force term in eq. (9) can be described as [44-46]:

$$F_i = 3w_i\beta[T(x,t) - T_m]\vec{g} \tag{10}$$

where T_m is the melting temperature and $T(x, t)$ is the temperature of liquid phase. The equilibrium function for the density distribution function for the D2Q9 model is given by [47]:

$$f_i^{eq} = w_i\rho\left[1 + \frac{3}{c^2}\vec{c}_i\vec{u} + \frac{9}{2c^4}(\vec{c}_i\vec{u})^2 - \frac{3}{2c^2}\vec{u}\vec{u}\right] \tag{11}$$

where u and ρ are the macroscopic velocity and density, respectively, and w_i is the weights to the velocity space discretization and represented as:

$$w_i = \begin{cases} \dfrac{4}{9} & i = 0 \\ \dfrac{1}{9} & i = 1,2,3,4 \\ \dfrac{1}{36} & i = 5,6,7,8 \end{cases} \tag{12}$$

In the present work, the velocity vector of particles for D2Q9 topology (fig. 2) is defined by:

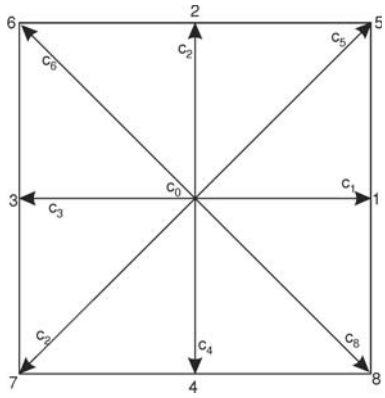

Figure 2. Discrete velocity set of 2-D nine-velocity (D2Q9) model

$$\vec{c}_i = \begin{cases} (0,0) \quad i = 0 \\ \left\{\cos\left[(i-1)\dfrac{\pi}{2}\right], \quad \sin\left[(i-1)\dfrac{\pi}{2}\right]\right\}c, \quad i = 1,\ 2,\ 3,4 \\ \sqrt{2}\left\{\cos\left[(2(i-5)+1)\dfrac{\pi}{4}\right], \quad \sin\left[(2(i-5)+1)\dfrac{\pi}{4}\right]\right\}c, \quad i = 5,\ 6,7,8 \end{cases} \tag{13}$$

In the above, $c = \Delta x/\Delta t$ is the particle streaming speed on the lattice, taken as $c = 1$ [45, 48] in most cases. Δx and Δt indicate the constant lattice apace and the time step, respectively.

The basic hydrodynamic quantities, such as density and velocity can be readily computed from the density distribution functions according to:

$$\rho = \sum_i f_i(x,t) \tag{14}$$

$$\rho\vec{u} = \sum_i \vec{c}_i f_i(x,t) \tag{15}$$

The viscosity of the fluid is related to the relaxation parameter τ by the eq. (16). The proof of these results follows from the Chapman-Enskog analysis which the details of this derivation are provided by Hou *et al.* [49]:

$$\nu = (\tau - 0.5)c_s^2\Delta t \tag{16}$$

The speed of sound, c_s, is a lattice-dependent quantity, which has the value of $c_s = c/3^{1/2}$ for the D2Q9 model. The positivity of the viscosity needs that the non-dimensional relaxation time must constantly be larger than 0.5.

LBE for the temperature field

In general, different LBM exist for treating heat transfer in a plain medium. In the present study, we select MDF approach [50, 51] to model melting with natural convection. It was stated [39, 52] that some limits such as the slight range of temperature difference, the numerical instability, and the constant value of the Prandtl number can be eliminated in the MDF model. The corresponding evolution equation of the temperature distribution function is also described by a BGK dynamic and is defined as:

$$g_i(x + c_i\Delta t, t + \Delta t) - g_i(x,t) = -\frac{1}{\tau_T}[g_i(x,t) - g_i^{eq}(x,t)] \tag{17}$$

where g_i is the temperature distribution function and τ_T is non-dimensional relaxation time for the temperature field. The equilibrium temperature distribution function can be given by [39]:

$$g_i^{eq} T w_i^T \left[1 + \frac{1}{c_s^2}(\vec{v}_i \vec{u})\right] \tag{18}$$

In this paper, the D2Q5 model for the evolution of g_i is employed. In this topology, the discrete velocity directions are:

$$\vec{v}_i = \begin{cases} (0,0) & i = 0 \\ \left\{\cos\left[(i-1)\frac{\pi}{2}\right], \quad \sin\left[(i-1)\frac{\pi}{2}\right]\right\} & i = 1,\ 2,\ 3,\ 4 \end{cases} \tag{19}$$

The associated weights, w_i^T are $w_0^T = 1/3$, $w_i^T = 1/6$ for $i = 1, 2, 3, 4$ and depend on the direction of the lattice velocity. The temperature, which is the relevant macroscopic variable, can be evaluated from:

$$T = \sum_{i=0}^{4} g_i \tag{20}$$

Through the Chapman-Enskog expansion, the energy equation can be exactly recovered from LBE. The thermal diffusivity is related to its dimensionless thermal relaxation time by eq. (21):

$$\alpha = \frac{c^2}{6}(2\tau_T - 12)\Delta t \tag{21}$$

Phase change treatment with LBM

As mentioned, there are two different LBM for solving solid-liquid phase change problems. A survey of phase change formulation demonstrates that the most common procedure observed in the solution of solid-liquid phase change problems has been the utilization of the enthalpy-based method. The benefit of employing the enthalpy method is that it removes the requirement of satisfying conditions at the phase change front. Hence, we apply the Jiaung *et al.* [36] melting scheme, which is an iterative enthalpy-based method, to solve both the temperature and liquid fraction. The total enthalpy is split into sensible and latent heat components in the vicinity of solid-liquid interface for phase-change problems.

The local enthalpy at the time step n and iteration k, is evaluated according to eq. (22) as:

$$En^{n,k} = c_p T^{n,k} + L_f f_l^{n,k-1} \tag{22}$$

The liquid fractions at the current iteration level are assumed to be:

$$f_l^{n,k} = \begin{cases} 0 & \text{if} \quad En^{n,k} < En_s \\ \dfrac{En^{n,k} - En_s}{En_l - En_s} & \text{if} \quad En_s \le En^{n,k} \le En_l \\ 1 & \text{if} \quad En^{n,k} > En_l \end{cases} \tag{23}$$

Then the temperature distribution functions are obtained by:

$$g_i^{n,k}(x + c_i\Delta t, t + \Delta t) = g_i(x,t) - \frac{1}{\tau_T}[g_i(x,t) - g_i^{eq}(x,t)] - w_i \frac{L_f}{c_p}(f_l^{n,k} - f_l^{n-1}) \tag{24}$$

Curved boundary

Figure 3 shows a part of an arbitrary curved wall geometry separating a solid region from fluid where the black small circles on the boundary x_w, the open circles represent the boundary nodes in the fluid region x_f and the grey solid circles indicate those in the solid region x_b.

In the boundary condition, both $f_i(x_b,t)$ and $g_i(x_b,t)$ are needed to perform the streaming steps on fluid nodes x_f. The fraction of an intersected link in the fluid region is Δ, that is,

$$\Delta = \frac{||x_f - x_w||}{||x_f - x_b||} \tag{25}$$

Obviously, $0 \le \Delta \le 1$. The standard (half-way) bounce back no-slip boundary condition always assumes a delta value of 0.5 to the boundary wall, fig. 4(a). Due to the curved boundaries, delta values in the interval of (0, 1) are now possible. Figure 4(b) shows the bounce back behavior of a surface with a delta value smaller than 0.5, and fig. 4(c) shows the bounce back behavior of a wall with delta bigger than 0.5.

In all three cases, the reflected distribution function at x_f is unknown. Since the fluid particles in the LBM are always considered to move one cell length per time step, the fluid particles would come to rest at an intermediate node x_i. In order to calculate the reflected distribution function in node x_f, an interpolation scheme has to be applied. For treating velocity field in curved boundaries, the method is based on the method reported in reference [53] while for handling tempera-

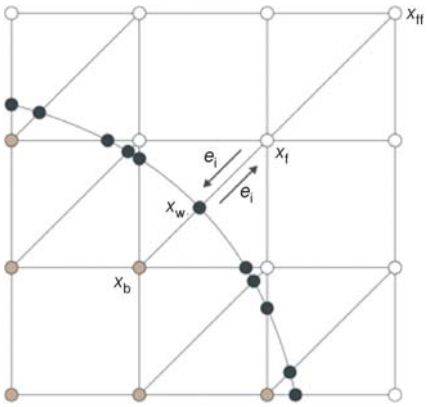

Figure 3. Curved wall boundary

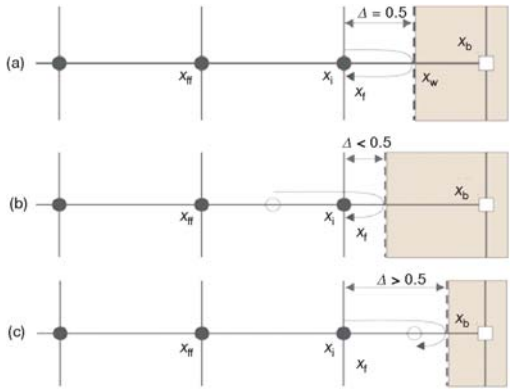

Figure 4. Illustration of the bounce-back boundary conditions. (a) Δ = 1/2, the perfect bounce-back without interpolation. (b) Δ < 1/2, the bounce-back with interpolations before the collision with the wall located at x_w. (c) Δ > 1/2, the bounce-back with interpolations after the collision with the wall

ture field the method is based on an extrapolation method of second-order accuracy applied in reference [54].

Velocity in curved boundary condition

To evaluate the distribution function in the solid region $f_i(x_b, t)$ based upon the boundary nodes in fluid region, the bounce-back boundary conditions combined with interpolations including a one-half grid spacing correction at the boundaries [51, 55]. Then the Chapman-Enskog expansion for the post-collision distribution function is conducted as:

$$f_i(x_\mathrm{b} + c_i\Delta t, t + \Delta t) = (1-\chi) f_i(x_\mathrm{f} + c_i\Delta t, t + \Delta t) + \chi f_i^*(x_\mathrm{b}, t) + 2\omega_i \frac{3}{c^2} e_i u_\mathrm{w} \tag{26}$$

where

$$f_i^*(x_\mathrm{b}, t) = f_i^{eq}(x_\mathrm{f}, t) + \omega_i \rho(x_\mathrm{f}, t) \frac{3}{c^2} e_i (u_\mathrm{bf} - u_\mathrm{f}) \tag{27}$$

$$u_\mathrm{bf} = u_\mathrm{ff} = u(x_\mathrm{ff}, t), \quad \chi = \frac{2\Delta - 1}{\tau - 2}, \quad \text{if} \quad 0 \le \Delta < \frac{1}{2} \tag{28a}$$

$$u_\mathrm{bf} = \frac{1}{2\Delta}(2\Delta - 3) u_\mathrm{f} + \frac{3}{2\Delta} u_\mathrm{w}, \quad \chi = \frac{2\Delta - 1}{\tau - \frac{1}{2}}, \quad \text{if} \quad \frac{1}{2} \le \Delta < 1 \tag{28b}$$

u_w denotes the velocity of solid wall, u_bf is the imaginary velocity for interpolations and $e_i \equiv -e_i$.

Temperature in curved boundary condition

To implement the curved boundary condition treatment for temperature, this study uses the method which is based on the method reported in reference [51]. The temperature distribution function can be divided into two parts: equilibrium and non-equilibrium:

$$g_i(x_\mathrm{b}, t) = g_i^{neq}(x_\mathrm{b}, t) + g_i^{eq}(x_\mathrm{b}, t) \tag{29}$$

By substituting eq. (29) into eq. (17) we have:

$$g_i(x_\mathrm{b} + c_i\Delta t, t + \Delta t) = g_i^{eq}(x_\mathrm{b}, t) + \left(1 - \frac{1}{\tau_\mathrm{T}}\right) g_i^{neq}(x_\mathrm{b}, t) \tag{30}$$

Obviously to calculate $g_i(x_\mathrm{b} + c_i\Delta t, t + \Delta t)$, both $g_i^{eq}(x_\mathrm{b}, t)$ and $g_i^{neq}(x_\mathrm{b}, t)$ are required. The equilibrium and non-equilibrium parts of eq. (29) are defined as:

$$g_i^{eq}(x_\mathrm{b}, t) = \omega_i^T T_b^* \left(1 + \frac{3}{c^2} e_i u_\mathrm{b}\right) \tag{31}$$

T_b^* is determined by linear extrapolation using either:

$$T_b^* = T_\mathrm{bl}, \quad \text{if} \quad \Delta \ge 0.75 \tag{32}$$

$$T_b^* = T_{b1} + (1 - \Delta) T_{b2}, \quad \text{if} \quad \Delta < 0.75 \tag{33}$$

where Δ is the fraction of the intersected link in the fluid region and:

$$T_{b1} = \frac{T_\mathrm{w} + (\Delta - 1) T_\mathrm{f}}{\Delta} \tag{34}$$

$$T_{b2} = \frac{2T_\mathrm{w} + (\Delta - 1) T_\mathrm{ff}}{1 + \Delta} \tag{35}$$

where T_f and T_{ff} denote the fluid temperature in node x_f and x_{ff}, respectively. The extrapolation scheme is the same as in ref. [56]. The next task is to determine $g_i^{neq}(x_b, t)$. Second-order approximation is also used. $g_i^{neq}(x_b, t)$ is calculated as:

$$g_i^{neq}(x_b, t) = \Delta g_i^{neq}(x_f, t) + (1-\Delta) g_i^{neq}(x_{ff}, t) \tag{36}$$

From the Chapman-Enskog analysis [57], $g_i^{neq}(x_b, t)$ can be expressed as:

$$g_i^{neq}(x, t) = g_i^1(x, t)\delta x \tag{37}$$

where $g_i^0(x, t)$ is the same order as $g_i^{eq}(x, t)$. Since $g_i^1(x_w, t) - g_i^1(x_f, t) = O(\delta x)$, $g_i^{neq}(x_w, t) - g_i^{neq}(x_f, t) = O(\delta x^2)$. By the same token, it can be proved that:

$$g_i^{neq}(x_w, t) - g_i^{neq}(x_{ff}, t) = O(\delta x^2) \tag{38}$$

That means the approximation $g_i^{neq}(x_b, t)$ is of second order in space which is in consistent with thermal LBE.

Code validation

A first validation was performed by comparing the results for a simple natural convection problem with a well-known benchmark solution [58]. The comparison is fulfilled at three different Ra = 10^4, 10^5, and 10^6 and its results shown in tab. 2. As it can be seen from tab. 2, the accuracy of present work in comparison with the benchmark solution of De Vahl Davis [58] is satisfying.

Table 2. The validation of the current results in a square cavity

	$\frac{u_{max}H}{\alpha}$	$\frac{v_{max}H}{\alpha}$	Nu_m
Ra = 10^4			
Benchmark [58]	16.187	19.617	2.243
Present work	15.71	20.15	2.2394
Ra = 10^5			
Benchmark [58]	34.730	68.590	4.519
Present work	35.54	70.341	4.56
Ra = 10^6			
Benchmark [58]	64.630	219.36	8.800
Present work	58.43	223.1	8.95

Figure 5(a) shows the average melt front position (S_{av}) as a function of dimensionless time, FoSte. The comparison between our numerical

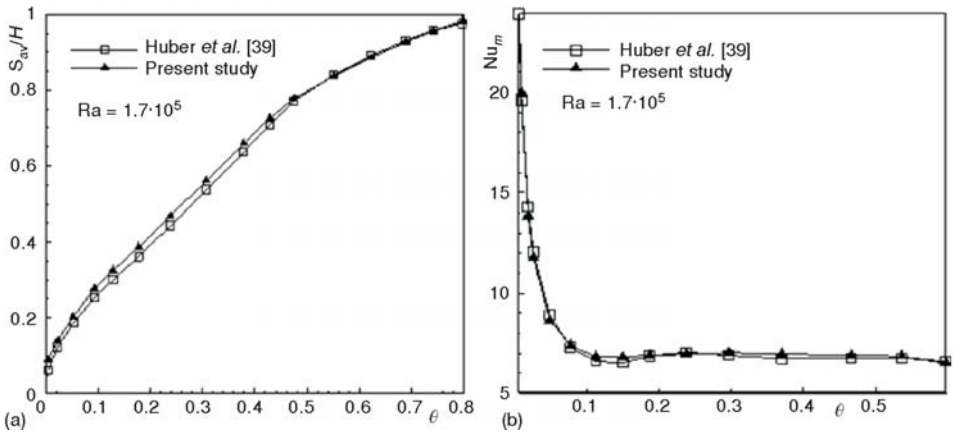

Figure 5. Comparison of average melting front position (a) and Nusselt number (b) *vs.* dimensionless time between present study and Huber *et al.* [39] work for Pr =1 and Ste = 10

results and Huber *et al.* [39] work is quite good. Figure 5(b) illustrates the comparison of the average Nusselt number at the left wall between present study and Huber *et al.* [39] work for Ra = $= 1.7 \cdot 10^5$, Pr =1, and Ste = 10. The present results are almost identical and quantitatively good agreement with ref. [39]. Different grid sizes were selected and tested to ensure the independency of solution from the adopted grid size based on comparison of melting fraction. The uniform square grid with the size of 200 × 200 was found suitable for the current condition.

Numerical results and discussion

Figure 6 shows the streamlines in an eccentric annulus for various dimensionless times. At the beginning of melting for any position of the inner cylinder, the pure conduction heat transfer dominates between inner cylinder and solid PCM. So, it causes to symmetric melting around inner cylinder. As time progresses, the warm liquid next to the hot inner cylinder rises upward and cold liquid next to the solid PCM replaces. Thus, a re-circulating vortex is formed between the solid PCM and hot inner cylinder after $\theta = 1.2 \cdot 10^{-4}$ and the shape of solid-liquid interface deviates from concentric pattern. For the cases of inner cylinder placed on the vertical symmetrical axis, the vortex splits into two symmetric re-circulating vortexes that demonstrate the equal strength of re-circulation on the both sides of the system. For the case of $X_r = 0$, $Y_r = 0.5$, the surface of outer cylinder plays a role like obstacle for further growing of these recirculating vortexes. So, the slight space on top region of the inner cylinder, restrains the circulation of the hot fluid. Conversely, when the inner cylinder shifts downward ($X_r = 0$, $Y_r = -0.5$), these two vortexes have enough space between surfaces of cylinders and can be further grown. As a result, the buoyancy-driven convection effect on melting process becomes more significant. When the inner cylinder is moved to the position of $X_r = -0.5$, $Y_r = 0$ or $X_r = -0.35$, $Y_r = -0.35$, two rotating vortexes form over both sides of the inner cylinder, the main (right) vortex and the secondary (left) vortex. This is because of the inhibition of secondary vortex growth at the small gap of left side and the domination of flow at the big gap of right side. Consequently, the size of these two vortexes completely depends on the gap spacing between two cylinders. It is remarkable to mention that, the centre of these vortexes placed at the upper half of the outer cylinder.

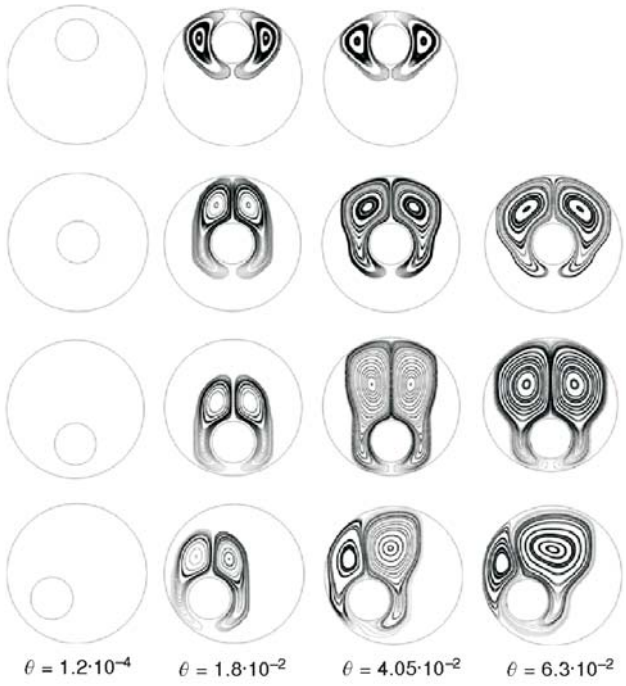

Figure 6. Streamlines for various dimensionless times for Ra of 10^5, Pr of 6.2, and Ste of 1

The distribution of temperature in the computational domain can be evidently observed from the colorized temperature contours shown in fig. 7. The dark (blue) portion of the temperature contours indicates the un-melted solid PCM. As can be seen, the melted PCM concentrates

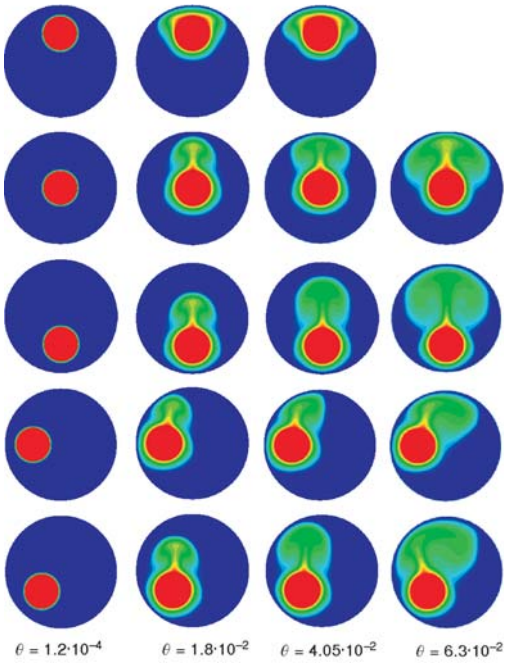

Figure 7. Temperature contours for various dimensionless times for Ra of 10^5, Pr of 6.2, and Ste of 1 (for color image see journal web site**)**

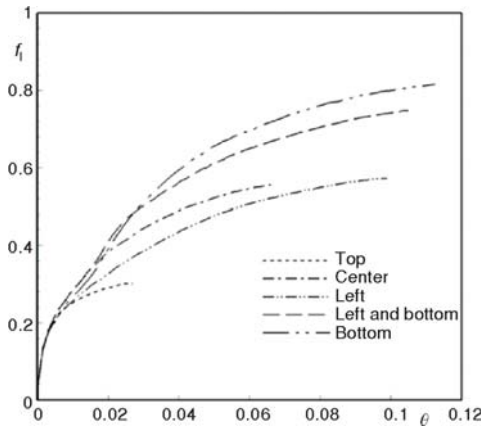

Figure 8. The variations of liquid fraction *vs.* dimensionless time for different positions of inner cylinder

on the top region of the outer cylinder because the convection heat transfer significantly dominates at this region.

The computed variations of liquid fraction against dimensionless time for different positions of the inner cylinder are plotted in fig. 8. The slopes of these graphs indicate the melting rate. The sharp slop of the graph at the beginning of the melting is due to direct contact between un-melted PCM and inner cylinder where the thickness of melted PCM is small.

Thus, conduction mode of heat transfer has great effect. As can be seen, the melting rates are approximately similar just before $\theta = 1.2{\cdot}10^{-4}$. During this time the conduction heat transfer dominates between inner cylinder and un-melted PCM. Also, it can be found that the maximum liquid fraction for top, center, left, left and bottom, and bottom positions of inner cylinder are 0.3, 0.55, 0.57, 0.74, and 0.81, respectively. So, the maximum of liquid fraction occurs where the inner cylinder is placed at the bottom.

Conclusions

The numerical simulation of melting phenomenon with natural convection in an eccentric annulus was carried out for Ra of 10^5, Pr of 6.2, Ste of 1, and radius ratio *rr* of 3.3. The LBM based on the combination of D2Q5 and D2Q9 models was applied for dealing with curved boundaries for thermal and flow features. The following conclusions can be drawn from the solution of this problem:

- LB numerical scheme based on the double-population is a very efficient numerical approach for simulating of melting phenomenon with natural convection in an eccentric annulus.
- As expected, the position of heated inner cylinder can significantly influence the flow pattern including the size and shape of two vortexes.
- Results show that the maximum of liquid fraction takes place where the inner cylinder is mounted at the bottom.

Nomenclature

c – streaming speed, [m]
$\vec{c}_i$ – discrete lattice velocity in direction i, [–]
c_p – heat capacity, [Jkg^{-1}K^{-1}]
c_s – speed of sound in lattice scale, [–]
En – enthalpy, [J]
En_l – enthalpy of the liquid phase, [J]
En_s – enthalpy of the solid phase, [J]
f_l – liquid fraction, [–]
f_k^{eq} – equilibrium distribution for velocity field, [–]
Fo – Fourier number ($\alpha t/l^2$), [–]
$\vec{g}$ – acceleration due to gravity, [ms^{-2}]
g_k^{eq} – equilibrium distribution for temperature field, [–]
g_k^{neq} – non-equilibrium distribution for temperature field, [–]
L_f – latent heat of phase change, [Jkg^{-1}]
l – appropriate length scale, [m]
Pr – Prandtl number (ν/α), [–]
R – radius of outer cylinder, [m]
Ra – Rayleigh number ($g\beta\Delta Tl^3/\alpha\nu$), [–]
r – radius of inner cylinder, [m]
rr – radius ratio (R/r), [–]
Ste – Stefan number [= $c_p(T_1 - T_0)/L_f$], [–]
T_l – temperature of inner cylinder, [K]
T_m – melting temperature of solid phase, [K]
T_0 – temperature of outer cylinder, [K]
Δt – lattice time step, [–]
w_i – equilibrium distribution weight, [–]
w_i^T – associated weight for temperature field, [–]
X_r, Y_r – dimensionless position of center of inner cylinder, [–]
Δx – lattice space, [–]

Greek symbols

α – thermal diffusivity, [m^{2}s^{-1}]
b – thermal expansion coefficient, [K^{-1}]
θ – dimensionless time [FoSte], [–]
ν – kinetic viscosity of the fluid, [m^{2}s^{-1}]
ρ – density, [kgm^{-3}]
τ – lattice relaxation time, [–]

Superscripts

i – direction
s – solid
l – liquid
r – inner cylinder

Superscripts

n – time step
k – iteration

References

[1] Benard, C., *et al.*, Melting in Rectangular Enclosures: Experiments and Numerical Simulations, *Journal of Heat Transfer, 107* (1985), 4, pp. 794-803
[2] Wolff, F., Viskanta, R., Melting of Pure Metal from a Vertical Wall, *Experimental Heat Transfer, 1* (1987), 1, pp. 17-30
[3] Wang, Y., *et al.*., An Experimental Investigation of the Melting Process in a Rectangular Enclosure, *International Journal of Heat and Mass Transfer, 42* (1999), 19, pp. 3659-3672
[4] Jany, P., Bejan, A., Scaling Theory of Melting with Natural Convection in an Enclosure, *International Journal of Heat and Mass Transfer, 31* (1988), 6, pp. 1221-1235
[5] Zhang, Z., Bejan, A., The Problem of Time-Dependent Natural Convection Melting with Conduction in the Solid, *International Journal of Heat and Mass Transfer, 32* (1989), 12, pp. 2447-2457
[6] Usmani, A. S., *et al.*, Finite Element Modelling of Natural-Convection-Controlled Change of Phase, *International Journal for Numerical Methods in Fluids, 14* (1992), 9, pp. 1019-1036
[7] Javierre, E., *et al.*, A Comparison of Numerical Models for One-Dimensional Stefan Problems, *Journal of Computational and Applied Mathematics, 192* (2006), 2, pp. 445-459
[8] Ng, K. W., *et al.*, Heat Transfer in Free Convection-Dominated Melting of a Phase Change Material in a Horizontal Annulus, *International Communications in Heat and Mass Transfer, 25* (1998), 5, pp. 631-640
[9] Betzel, T., Beer, H., Solidification and Melting Heat Transfer to an Unfixed Phase Change Material (PCM) Encapsulated in a Horizontal Concentric Annulus, *Heat and Mass Transfer, 22* (1988), 6, pp. 335-344
[10] Khillarkar, D. B., *et al.*., Melting of a Phase Change Material in Concentric Horizontal Annuli of Arbitrary Cross-Section, *Applied Thermal Engineering, 20* (2000), 10, pp. 893-912
[11] Liu, Z., *et al.*, Experimental Investigations on the Characteristics of Melting Processes of Stearic Acid in an Annulus and its Thermal Conductivity Enhancement by Fins, *Energy Conversion and Management, 46* (2005), 6, pp. 959-969

[12] Dutta, R., *et al.*, Experimental and Numerical Study of Heat Transfer in Horizontal Concentric Annulus Containing Phase Change Material, *The Canadian Journal of Chemical Engineering, 86* (2008), 4, pp. 700-710
[13] Tombarevic, E., Vusanovic, I., Modeling of Ice-Water Phase Change in Horizontal Annulus Using Modified Enthalpy Method, *Advances in Applied Mathematics and Mechanics, 3* (2011), 3, pp. 354-369
[14] Rabienataj Darzi, A. A., *et al.*, Numerical Study of Melting Inside Concentric and Eccentric Horizontal Annulus, *Applied Mathematical Modelling, 36* (2012), 9, pp. 4080-4086
[15] Bertrand, O., *et al*., Melting Driven by Natural Convection, a Comparison Exercise: First Results, *International Journal of Thermal Sciences, 38* (1999), 1, pp. 5-26
[16] Tan, L., Zabaras, N., A Level Set Simulation of Dendritic Solidification with Combine Features of Front-Tracking and Fixed-Domain Methods, *Journal of Computational Physics, 211* (2006), 1, pp. 36-63
[17] Jin, C., Xu, K., An Adaptive Grid Method for Two-Dimensional Viscous Flows, *Journal of Computational Physics, 218* (2006), 1, pp. 68-81
[18] Boettinger, W. J., *et al*., Phase-Field Simulation of Solidification, *Annual Review of Materials Research, 32* (2002), 8, pp. 163-194
[19] Wang, C.-C., *et al*., Application of Lattice Boltzmann Method and Field Synergy Principle to the Heat Transfer Analysis of Channel Flow with Obstacles Inside, *Thermal Science, 15* (2011), 1, pp. 75-80
[20a] Yan, Y. Y., Zu, Y. Q., Numerical Simulation of Heat Transfer and Fluid Flow Past a Rotating Isothermal Cylinder – A LBM Approach, *International Journal of Heat and Mass Transfer, 51* (2008), 9-10, pp. 2519-2536
[20b] Fattahi, E., *et al.*, Lattice Boltzmann Simulation of Natural Convection Heat Transfer in Eccentric Annulus, *International Journal of Thermal Sciences, 49* (2010), 12, pp. 2353-2362
[21] Azwadi, C. S. N., *et al.*, Lattice Boltzmann Simulation of Plume Behaviour from an Eccentric Annulus Cylinder, *International Journal of Mechanical and Materials Engineering, 5* (2010), 2, pp. 129-135
[22] Fattahi, E., *et al.*, Lattice Boltzmann Simulation of Mixed Convection Heat Transfer in Eccentric Annulus, *International Communications in Heat and Mass Transfer, 38* (2011), 8, pp. 1135-1141
[23] Jourabian, M., *et al*., Melting of NEPCM within a Cylindrical Tube: Numerical Study Using the Lattice Boltzmann Method, *Numerical Heat Transfer, Part A, 61* (2012), 12, pp. 929-948
[24] Nemati, H., *et al*., Lattice Boltzmann Simulation of Nanofluid in Lid-Driven Cavity, *International Communications in Heat and Mass Transfer, 37* (2010), 10, pp. 1528-1534
[25] Fattahi, E., *et al*., Lattice Boltzmann Simulation of Natural Convection Heat Transfer in Nanofluids, *International Journal of Thermal Sciences, 52* (2012), 2, pp. 137-144
[26] Semma, E., *et al*., Investigation of Flows in Solidification by Using the Lattice Boltzmann Method, *International Journal of Thermal Sciences, 47* (2008), 3, pp. 201-208
[27] Semma, E., *et al.*, Lattice Boltzmann Method for Melting/Solidification Problems, *Comptes Rendus Mécanique, 335* (2007), 5-6, pp. 295-303
[28] Ganaoui, M. El., Semma, E. A., A Lattice Boltzmann Coupled to Finite Volumes Method for Solving Phase Change Problems, *Thermal Science, 13* (2009), 2, pp. 205-216
[29] Gao, D., Chen, Z., Lattice Boltzmann Simulation of Natural Convection Dominated Melting in a Rectangular Cavity Filled with Porous Media, *International Journal of Thermal Sciences, 50* (2011), 4, pp. 493-501
[30] Gong, S., Cheng, P., A Lattice Boltzmann Method for Simulation of Liquid-Vapor Phase-Change Heat Transfer, *International Journal of Heat and Mass Transfer, 55* (2012), 17-18, pp. 4923-4927
[31] Eshraghi, M., Felicelli, S. D., An Implicit Lattice Boltzmann Model for Heat Conduction with Phase Change, *International Journal of Heat and Mass Transfer, 55* (2012), 9-10, pp. 2420-2428
[32] Miller, W., *et al.*, Lattice Boltzmann Model for Anisotropic Liquid-Solid Phase Transition, *Physical Review Letters, 86* (2001), 16, pp. 3578-3581
[33] Miller, W., Succi, S., A Lattice Boltzmann Model for Anisotropic Crystal Growth from Melt, *Journal of Statistical Physics, 107* (2002), 1-2, pp. 173-186
[34] Rasin, I., *et al.*, Phase-Field Lattice Kinetic Scheme for the Numerical Simulation of Dendritic Growth, *Physical Review E, 72* (2005), 6, pp. 1-10
[35] Medvedev, D., Kassner, K., Lattice Boltzmann Scheme for Crystal Growth in External Flows, *Physical Review E, 72* (2005), 6, pp. 1-10
[36] Jiaung, W. S., *et al.*, Lattice-Boltzmann Method for the Heat Conduction Problem with Phase Change, *Numerical Heat Transfer: Part B, 39* (2001), 6, pp. 167-187

[37] Chatterjee, D., Chakraborty, S., An Enthalpy-Based Lattice Boltzmann Model for Diffusion Dominated Solid-Liquid Phase Transformation, *Physics Letters A, 341* (2005), 1-4, pp. 320-330
[38] Chatterjee, D., Chakraborty, S., An Enthalpy-Source Based Lattice Boltzmann Model for Conduction Dominated Phase Change of Pure Substances, *International Journal of Thermal Sciences, 47* (2008), 5, pp. 552-559
[39] Huber, C., *et al*., Lattice Boltzmann Model for Melting with Natural Convection, *International Journal of Heat and Fluid Flow, 29* (2008), 5, pp. 1469-1480
[40] Bodenschatz, E., *et al.*, Recent Developments in Rayleigh-Benard Convection, *Annual Review of Fluid Mechanics, 32* (2000), 1, pp. 709-778
[41] Benzi, R., *et al.*., The lattice Boltzmann Equation: Theory and Applications, *Physics Reports, 222* (1992), 3, pp. 145-197
[42] Chen, S., Doolen, G. D., Lattice Boltzmann Method for Fluid Flows, *Annual Review of Fluid Mechanics, 30* (1998), 1, pp. 329-364
[43] Succi, S., *Lattice Boltzmann Method for Fluid Dynamics and Beyond*, Oxford, UK, 2001
[44] Djebali, R., *et al*., Some Benchmarks of a Side Wall Heated Cavity Using Lattice Boltzmann Approach, *Fluid Dynamics & Material Processing (FDMP), 5* (2009), 3, pp. 261-282
[45] Mohamad, A. A., *et al.*, Lattice Boltzmann Simulation of Natural Convection in an Open Ended Cavity, *International Journal of Thermal Sciences, 48* (2009), 10, pp. 1870-1875
[46] Rabienataj Darzi, A. A., *et al*., Mixed Convection Simulation of Inclined Lid Driven Cavity Using Lattice Boltzmann Method, *Iranian Journal of Science and Technology, Transection B, 35* (2011), M1, pp. 209-219
[47] He, X., *et al.*, A Novel Thermal Model for the Lattice Boltzmann Method Incompressible Limit, *Journal of Computational Physics, 146* (1998), 6, pp. 282-300
[48] Lallemand, P., Luo, L. S., Lattice Boltzmann Method for Moving Boundaries, *Journal of Computational Physics, 184* (2003), 2, pp. 406-421
[49] Hou, S., *et al*., Simulation of Cavity Flow by the Lattice Boltzmann Method, *Journal of Computational Physics, 118* (1995), 2, pp. 329-347
[50] Shan, X., Simulation of Rayleigh-Benard Convection Using a Lattice Boltzmann Method, *Physical Review E, 55* (1997), 2, pp. 2780-2788
[51] Guo, Z., *et al.*, A Coupled Lattice BGK Model for the Boussinesq Equations, *International Journal for Numerical Methods in Fluids, 39* (2002), 4, pp. 325-342
[52] Guo, Z., Zhao, T. S., A Lattice Boltzmann Model for Convection Heat Transfer in Porous Media, *Numerical Heat Transfer, Part B, 47* (2005), 2, pp. 157-177
[53] Guo, Z. L., *et al.*, An Extrapolation Method for Boundary Conditions in Lattice Boltzmann Method, *Physics of Fluids, 14* (2002), 6, pp. 2007-2010
[54] Mei, R., *et al*., Force Evaluation in the Lattice Boltzmann Method Involving Curved Geometry, *Physical Review E, 65* (2002), 4, pp. 1-14
[55] Yu, D., *et al*., Viscous Flow Computations with the Method of Lattice Boltzmann Equation, *Progress in Aerospace Sciences, 39* (2003), 5, pp. 329-367
[56] Glapke, E. K., *et al.*, Constant Heat Flux Solutions for Natural Convection between Concentric and Eccentric Horizontal Cylinders, *Numerical Heat Transfer, 10* (1986), 3, pp. 279-295
[57] Yuan, P., Laura, S., A Thermal Lattice Boltzmann Two-Phase Flow Model and its Application to Heat Transfer Problems – Part 1, Theoretical Foundation*, Journal of Fluids Engineering, 128* (2006), 1, pp. 142-150
[58] Vahl Davis, G. D., Natural Convection of Air in a Square Cavity: A Benchmark Numerical Solution, *International Journal for Numerical Methods in Fluids, 3* (1983), 4, pp. 249-264

Paper submitted: May 10, 2011
Paper revised: November 3, 2012
Paper accepted: February 19, 2013